



CHORUS

This is the accepted manuscript made available via CHORUS. The article has been published as:

Anisotropic Diffusion of a Charged Tritium Interstitial in $\text{Li}_{\{2\}}\text{TiO}_{\{3\}}$ from First-Principles Calculations

Yanli Shi, Jianqi Qi, Yong Han, and Tiecheng Lu

Phys. Rev. Applied **10**, 024021 — Published 16 August 2018

DOI: [10.1103/PhysRevApplied.10.024021](https://doi.org/10.1103/PhysRevApplied.10.024021)

Anisotropic diffusion of a charged tritium interstitial in Li_2TiO_3 from first-principles calculations

Yanli Shi,^{1,2} Jianqi Qi,^{1,3} Yong Han,^{4,5,*} and Tiecheng Lu^{1,2,†}

¹College of Physical Science and Technology, Sichuan University, Chengdu 610064, Sichuan, P. R. China

²Key Laboratory of Radiation Physics and Technology of Ministry of Education, Sichuan University, Chengdu 610064, Sichuan, P. R. China

³Key Laboratory of High Energy Density Physics of Ministry of Education, Sichuan University, Chengdu 610064, Sichuan, P. R. China

⁴Ames Laboratory, U. S. Department of Energy, Iowa State University, Ames, Iowa 50011, United States

⁵Department of Physics and Astronomy, Iowa State University, Ames, Iowa 50011, United States

Tritium diffusion in the nuclear fusion reactor breeder material Li_2TiO_3 is a fundamentally important process for the tritium release kinetics. The energy barrier of tritium diffusion in Li_2TiO_3 was reported with a considerable uncertainty in previous experiments. Here, we perform the systematic density-functional-theory (DFT) studies for the diffusion processes of a positively-charged tritium, which is the most preferable charge state of the tritium interstitial in a single Li_2TiO_3 crystal. By calculating various local-diffusion minimum-energy paths, we find that the diffusion of the tritium is strongly anisotropic along different crystalline directions. The most favorable diffusion paths appear within a Li_6 atomic single layer of Li_2TiO_3 and the corresponding DFT diffusion barrier is 0.334 eV, while the diffusion barrier for most favorable diffusion paths crossing a Li_2Ti_4 atomic layer is 1.006 eV.

*y27h@ameslab.gov

†lutiecheng@scu.edu.cn

I. INTRODUCTION

In prospective nuclear fusion reactors, energy supply is expected to be gained greatly from the deuterium-tritium (D-T) reaction, ${}^2_1\text{D} + {}^3_1\text{T} \rightarrow {}^4_2\text{He} + {}^1_0\text{n}$, where deuterium and tritium are as the fuel [1]. Deuterium can be easily extracted from the sea water, while tritium must be obtained via the lithium-neutron reaction using the neutrons released from the D-T reaction. Lithium is provided by lithium-based breeder materials which are placed in the blanket module surrounding the fusion chamber. Tritium recovery efficiency is the primary concern for the breeder material because this determines if the D-T reaction is sustainable. In addition, a breeder material demands to withstand severe radiation-induced damage and high temperatures, as well as to be compatible with the structural material. Lithium titanate (Li_2TiO_3) has been chosen as the ceramic material in multiple blanket designs where the solid-state breeders are used [2]. Relative to all other candidates (such as Li_2O , Li_4SiO_4 , Li_2ZrO_3 , LiAlO_2 , etc.) of breeder ceramics, Li_2TiO_3 has reasonable lithium density, high melting temperature, low activation, good chemical stability, nice structure compatibility, and excellent tritium release performance, therefore Li_2TiO_3 being considered as a very promising breeder material in fusion reactors [3-7].

In breeder ceramics, tritium is first generated in crystal grains. To be transported out of the ceramic and released into the purge gas, tritium needs to go through two basic processes: one is the diffusion in the bulk, and another one is the desorption from the surface [8]. Therefore, the extraction rate is controlled by both the diffusion and the desorption mechanism. It has been found that, in larger grains and under elevated temperatures, diffusion is the rate-limiting mechanism, while in other situations, the rate-limiting mechanism switches to desorption [9, 10]. The detrapping process from irradiation defects is also found to play a part in the diffusion mechanism, and the activation energy for detrapping is notably higher [11]. From a series of studies of tritium release in Li_2TiO_3 , the activation energy of tritium diffusion is estimated to be in the range of 0.4 to 1.6 eV with a considerable uncertainty under different temperatures and in various Li_2TiO_3 samples [11-17].

As the initial step of the tritium release process, tritium transport in crystal grains may largely determine the final extraction rate. In the Li_2TiO_3 grain, tritium is either incorporated as an interstitial defect or trapped in intrinsic defects. It has been discovered that both lithium and oxygen vacancies can trap tritium. Tritium trapped in a lithium vacancy (V_{Li}) tends to move away from the vacancy center and is bound to nearby oxygen ions forming hydroxyl groups [18, 19]. In addition, the neutrally-charged tritium- V_{Li} defects are predicted to be the most dominant tritium-containing defects in TiO_2 -rich Li_2TiO_3 [20]. Oyaudzu *et al.* conclude that tritium release is triggered by annihilation of irradiation-induced defects, and the major tritium release occurs directly after the annihilation of oxygen vacancies (V_{O}),

while no obvious tritium release is related to the annihilation of V_{Li} [21]. V_{O} trapping is predicted to be a major form of tritium incorporation at low-oxygen partial pressures [20]. If not trapped in intrinsic defects, tritium is incorporated as an interstitial defect. The most probable sites of tritium interstitials are found to be at the Li-O interlayers in Li_2TiO_3 , and such interstitial defects are more favorable than V_{Li} trapping [22, 23]. Additionally, the most preferable charge state of the tritium interstitial is +1, and the interstitial defect structure is tritium bonding to the nearby oxygen ion forming a hydroxyl group [20].

The lithium ion diffusion in Li_2TiO_3 has been studied both by experiments and simulations [24, 25]. The lithium ion diffusion paths were determined by combining molecular dynamics simulations and a nudged-elastic-band method within an empirical potential [25]. The tritium diffusion in Li_2TiO_3 as a crucial process during the tritium release, however, has not yet been reported so far. In this work, we present an extensive first-principles density-functional-theory (DFT) study for locally-stable tritium interstitial sites in Li_2TiO_3 and the diffusion of tritium between these sites. We focus on the diffusion of tritium as an interstitial defect in the Li_2TiO_3 crystal neglecting the influence of intrinsic defects. We use the climbing nudged-elastic-band (cNEB) method [26, 27] to obtain minimum energy paths (MEPs) of tritium diffusion between two interstitial sites. From the MEPs, we determine the corresponding diffusion barrier (i.e., activation energy), the key quantity for analyzing, modeling, and simulating the tritium migration behavior in the Li_2TiO_3 crystal.

In Sec. II, we describe the crystal structure of Li_2TiO_3 , DFT method used in our calculations, and model analysis for simulating the tritium diffusion in the Li_2TiO_3 crystal. In Sec. III, we first determine possible locally-stable sites for tritium interstitials in Li_2TiO_3 and compare our DFT results with those available from previous literature. Then, we show and discuss the various local diffusion paths and corresponding diffusion barriers of tritium interstitials from our extensive first-principles DFT calculations. Having these local diffusion paths, we analyze the long-range anisotropic diffusion paths along any different crystalline directions. Finally, in Sec. VII, we make a summary.

II. CRYSTAL STRUCTURE OF Li_2TiO_3 , DFT METHOD, AND MODEL

In this work, we focus on the monoclinic β -phase Li_2TiO_3 , which is stable throughout the operating temperature range of a breeder material [28, 29]. The single-crystal Li_2TiO_3 can be characterized by a $C2/c$ space group with lattice parameters: $a = 0.50623$ nm, $b = 0.87876$ nm, $c = 0.97533$ nm, and $\beta = 100.212^\circ$, determined experimentally at 295 K by Kataoka, *et al.* [28]. The crystal structure of Li_2TiO_3 features the stacking sequence $-(\text{Li}_6-\text{O}_6-\text{Li}_2\text{Ti}_4-\text{O}_6)-$ along the $\langle 001 \rangle$ direction. In Sec. III A, we will describe more details of each atomic layer in the

stacking sequence.

We perform all DFT calculations using the plane-wave-based Vienna *ab initio* simulation package (VASP) code [30, 31]. The projector augmented-wave (PAW) method [32] is utilized for the electron-core interactions with the pseudopotentials generated by the VASP group. The Perdew-Burke-Ernzerhof (PBE) generalized gradient approximation (GGA) [33] as the electronic exchange-correlation energy functional is implemented. The PBE-GGA functional has been recently used by Murphy to calculate the various defect formation energies in Li_2TiO_3 . [20]

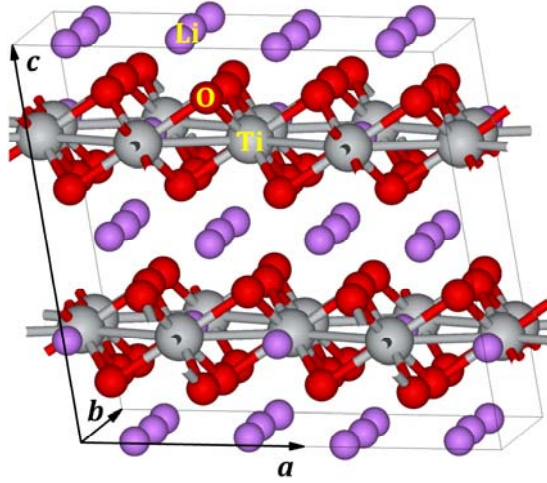


FIG. 1. The DFT-optimized $2\times 1\times 1$ supercell used to calculate tritium diffusion in the Li_2TiO_3 crystal. The types of atoms as well as the primitive translation vectors \mathbf{a} , \mathbf{b} , and \mathbf{c} are indicated. The angle between \mathbf{a} and \mathbf{c} is β , while \mathbf{a} and \mathbf{b} , or \mathbf{b} and \mathbf{c} , are perpendicular to each other.

In our DFT calculations, we use a $2\times 1\times 1$ supercell (in units of the primitive translation vectors \mathbf{a} , \mathbf{b} , and \mathbf{c}), which is sufficiently large to eliminate the error caused by the Coulomb interaction between charged defects in the periodic replicas (for the supercell-size testing details, see Sec. S1 [34]). Based on the results of convergence tests, the energy cutoff for the plane-wave basis is set to be 400 eV, and the Brillouin zone is sampled by a $3\times 2\times 2$ G-centered mesh. The geometry relaxation is considered to be completed when the total force on any atom is less than 0.1 eV/nm. The initial supercell is subjected to a full geometry optimization, and the obtained lattice constants of the supercell are $a = 0.5039$ nm, $b = 0.8743$ nm, $c = 0.9653$ nm, and $\beta = 100.2^\circ$, which are in good agreement with the above experimental values. Figure 1 shows the optimized supercell, which will be used in our DFT calculations for tritium diffusion.

In this work, we always treated tritium as hydrogen because modifying the mass in the standard pseudopotential for hydrogen to obtain the pseudopotential for

isotopes (deuterium or tritium) of hydrogen does not affect the electronic properties. Tritium diffusion in the Li_2TiO_3 crystal is modeled by the jump of a hydrogen interstitial between two adjacent sites. Recently, Murphy [20] has concluded that T^+ (tritium with a positive charge) is the most dominant charge state for the tritium interstitial in Li_2TiO_3 , and thus we always consider a tritium interstitial to be a T^+ in our calculations. The system of Li_2TiO_3 containing a T^+ is modeled by Li_2TiO_3 plus a H^+ , i.e., adding one hydrogen atom in Li_2TiO_3 and simultaneously removing one electron. It has been known that nuclear quantum effects (NQEs) may be significantly large for a system with diffusing hydrogen, e.g., NQEs can augment the delocalization of a proton in the hydrogen-bonded network [35] and therefore decrease transfer barriers more than reorientation barriers. Here we consider T^+ (not proton), and then the NQEs are assumed to be weaker and thus not taken into account in this work. In fact, recently Wilkins *et al.* [36] have provided a molecular description of the NQEs on water reorientation and hydrogen-bond dynamics in liquid H_2O and heavy water (D_2O), showing that the net NQE leads to an acceleration of about 13% in H_2O dynamics in contrast to a classical description, while it is negligible in D_2O .

To be obtain MEPs of tritium diffusion, locally-stable sites of tritium interstitials (hereinafter referred to as “T sites” for short) need to be determined first. Here it is necessary to make a note that sometimes a site is not at a local energy minimum, but there is a very flat potential-energy surface (PES) near it, and therefore such site is also identified as a T site for convenience of the cNEB calculations, as will be described in Sec. III. Previous studies have shown that tritium interstitials most likely stay between Li-O interlayers, and bonded to the O atoms [20, 22, 23]. Thus, we search the T sites around an O atom by relaxing all atoms after initially separately placing the tritium interstitial at multiple sites with a typical O-H bond length. To compare the stabilities of the interstitials at different local sites, we calculate the formation energy of the charged defect as [37, 38, 39]

$$E_f = E_{\text{tot}} - E_0 - \mu_{\text{T}} + \varepsilon_{\text{F}}, \quad (1)$$

where E_{tot} is the total energy of the system of Li_2TiO_3 plus tritium, E_0 is the energy of the defect-free system (i.e., the bulk Li_2TiO_3 crystal without tritium), μ_{T} represents the chemical potential of tritium which is calculated by halving the energy of a H_2 molecule in gas phase, and ε_{F} is the energy of removing the electron to form the charge state. ε_{F} can be also expressed as $\varepsilon_{\text{F}} = E_{\text{F}} - E_{\text{VBM}}$, where E_{F} is the Fermi energy (defined as the energy of an electron at the Fermi level), and E_{VBM} is the energy of the valence band maximum (VBM) of the defect-free system, that is to say, ε_{F} is the Fermi energy relative to E_{VBM} .

Once all the T sites are determined, we can perform the cNEB calculations for all possible diffusion paths between any two adjacent T sites. Then, we obtain the MEP and therefore diffusion barrier which is defined as the energy difference

between the highest-energy saddle point and an endpoint on the MEP. The choice of the number of cNEB images for MEP convergence is remarked in Sec. S1 [34].

III. RESULTS AND DISCUSSION

A. T sites and formation energies

From Fig. 2(a), the $2 \times 1 \times 1$ supercell is composed of four O_6 layers, two Li_6 layers, and two Li_2Ti_4 layers along the $\langle 001 \rangle$ direction. In a $1 \times 1 \times 1$ cell, which is the half along the $\langle 100 \rangle$ direction of the above $2 \times 1 \times 1$ supercell, each O_6 (Li_6) layer contains six O (Li) atoms, and each Li_2Ti_4 layer contains two Li plus four Ti atoms, as shown in Fig. 1. The periodic stacking sequence of O_6 , Li_6 , and Li_2Ti_4 layers are also indicated by dashed lines in Fig. 2(a). As mentioned in Sec. II, all the T sites will be determined around the positions of O atoms from our DFT calculations. By fully relaxing the geometries with tritium around the O atoms, we find that there are six nonequivalent T sites, and tritium at each T site is bonded to a nearby O atom. The T sites in the supercell are indicated by the small white balls in Fig. 2(a).

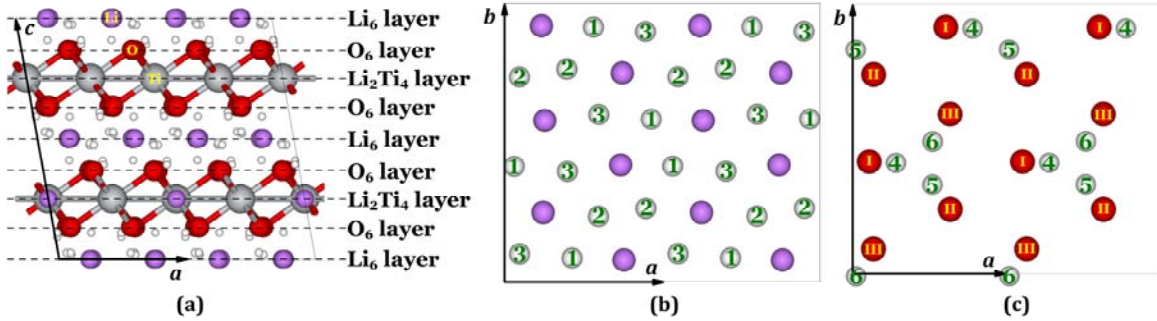


FIG. 2. (a) The $2 \times 1 \times 1$ supercell (solid frame) viewed along the $\langle 010 \rangle$ direction. The atomic monolayers in the stacking sequence $-(Li_6-O_6-Li_2Ti_4-O_6)-$ along the $\langle 001 \rangle$ direction is indicated by the dashed lines. Small white balls represent the T sites. (b) A single Li_6 layer and nearby T sites (labelled as 1, 2, and 3), viewed along the $\langle 001 \rangle$ direction. (c) A single O_6 layer and nearby T sites (labelled as 4, 5, and 6), viewed along the $\langle 001 \rangle$ direction. Three nonequivalent O atoms (O_I , O_{II} , and O_{III}) are also labeled.

For convenience of discussion, we classify the above six nonequivalent T sites according to their positions. Three nonequivalent T sites very close to the Li_6 layer (see Fig(a)) are called “ Li_6 -layer T sites” for simplicity. Each Li_6 -layer T site is approximately at the center of a triangle constructed by three nearest-neighboring (NN) Li atoms in a Li_6 layer, and these three Li_6 -layer T sites are identified as the numbers 1, 2, and 3, respectively (see Fig. 2(b)). In addition, all O-T bonds for these three Li_6 -layer T sites are roughly perpendicular to the O_6 layer. Similarly, the other three nonequivalent T sites are near the O_6 layer and therefore called “ O_6 -layer T sites”. These three O_6 -layer T sites are identified as the numbers 4, 5, and 6,

respectively (see Fig. 2(c)). All O-T bonds for these three O₆-layer T sites are almost parallel to the O₆ layer. We also identify three O atoms near the T sites 4, 5, and 6 as O_I, O_{II}, and O_{III}, respectively (see Fig. 2(c) again). Note that, for a Li₆-O₆ layer (i.e., a Li₆ layer plus its NN O₆ layer), T sites 1 and 4 are bonded to O_I, T sites 2 and 5 are bonded to O_{II}, and T sites 3 and 6 are bonded to O_{III}.

By analyzing the electronic structure for the relaxed geometry, we can see the sp^3 hybridized O atoms. Two of four sp^3 hybrid orbitals are used to form bonds to the two NN Ti atoms, and other two sp^3 hybrid orbitals hold the two lone pairs of electrons. Four orbitals construct a slightly-distorted tetrahedron. The T⁺ ion can take either of the two lone-pair orbitals to form an O-T bond, and this therefore explains why the two possible T sites are bonded to each O atom.

TABLE I. Formation energies (at the VBM), O-T bond lengths, and Bader charges of tritium at T sites from our DFT calculations. The energies relative to the T site 1 are listed to be compared with previously-reported values.

Position	T sites	E_f (eV)	O-T bond length (nm)	Charge (e)	Relative energy (eV)	
					This work	Reported value [20]
Li ₆ layer	1	-3.423	0.0982	0.41	0.000	0.00
	2	-3.422	0.0981	0.37	0.002	0.01
	3	-3.253	0.0984	0.44	0.170	0.18
O ₆ layer	4	-3.328	0.0980	0.41	0.095	0.09
	5	-3.333	0.0980	0.38	0.090	0.09
	6	-3.254	0.0983	0.43	0.169	0.15

The formation energies E_f calculated from Eq. (1) for the Fermi level at the VBM are listed in Table 1. The E_f values at the six T sites with lowest energies are in the range from -3.423 to -3.254 eV, which have different absolute values from the previously-reported results by Murphy due to the choice of a different energy reference [20]. However, the relative energies at the six T sites from our calculations are in good agreement with the results from Murphy (see Table 1). We also note that Murphy [20] has identified a seventh site (labeled as 91 in Table 2 of Ref. [20], where the subscript of notation for the defect should be “7” instead of the possible typo “6”), at which the energy is at least 90 meV higher than those at the other six T sites. We cannot find this seventh site, and therefore do not consider such a site in the calculations for tritium diffusion below. In addition, from our cNEB calculations, we find that the T site 4 or 5 in Table 1 is not an energy minimum, and instead a cusp with a very flat and a steeper PES on its two sides near it, respectively (for details, see Secs. III B and III C).

We also list the O-T bond lengths and Bader charges [40] of tritium at the six T sites in Table 1. All O-T bond lengths are almost the same in the range from 0.0980 to 0.0984 nm. The positively-charged tritium ions have the Bader charges from 0.37 e to 0.44 e , where e is the elementary charge.

From Table 1, the energies at T sites 3 and 6 bonded O_{III} are relatively much higher than at the other four T sites, and thus tritium jumps towards these two sites are thermodynamically unfavorable. By examining O-Ti bond lengths, we find that O_{III}-Ti has slightly longer bond lengths than both O_I-Ti and O_{II}-Ti, and therefore O_{III} atoms are slightly closer to the Li₆ layer than O_I and O_{II} atoms. This subtle geometric difference in bond length is perhaps related to the much higher energies of the T sites near O_{III}. In addition, there are almost the same energies and O-T bond lengths at T sites 1 and 2 (or 4 and 5), but the Bader charges have the noticeable difference (see Table 1), indicating the nonequivalence of O_I and O_{II}. The Bader charges at the T sites 1 and 4 bonded to O_I (or 2 and 5 bonded to O_{II}, or 3 and 6 bonded to O_{III}) are almost the same, but the energies are very different. Finally, because the energies at T sites 1 and 2, which are near the Li₆ layers, are lowest (i.e., T sites 1 and 2 are most favorable thermodynamically for trapping tritium than other T sites), we can predict that the Li₆ layers should have more population of tritium than the O₆ layers.

B. Local diffusion paths and energy barriers

To ultimately obtain long-range favorable diffusion paths of tritium interstitials, we first calculate various possible local diffusion paths between two NN T sites in the lattice made up of these T sites. Unlike the lattice of a usual crystal, the distances between two NN T sites are not a constant, as shown in Fig. 2 as well as listed in Table 2. Therefore, these T sites resemble the vertex set in graph theory, and the T-site lattice resembles an edge set (or a complex network [41]), where each edge joins an unordered pair of vertices (i.e., T sites). In general, the number of MEPs between two NN T sites corresponding to an edge can be more than one. When we say the MEP corresponding to an edge between two T sites in the text below, it means the most favorable MEP (i.e., that one with lowest diffusion barrier and shortest range) unless it is specifically explained.

For some edges, we can normally obtain an *independent* MEP by performing a simple cNEB calculation. However, the straightforward diffusion processes for some edges are precluded due to the existence of some Li, O, or Ti atoms between the T sites. In this case, a MEP corresponding to an edge can be obtained by connecting some of the above independent MEPs, and therefore is *dependent*. From our extensive cNEB calculations, we find that the number of the independent local MEPs (ILMEPs) corresponding to different edges is thirteen, which is smaller than the total number of edges. Thus, these thirteen ILMEPs are the components of any one dependent local MEP or any one long-range MEP, as will be discussed below as well

as in Sec. III C. For convenience, we classify these ILMEPs as three classes: C1, C2, and C3. Class C1 includes six ILMEPs for the diffusion within a Li_6 layer, class C2 includes three ILMEPs for the diffusion between a Li_6 layer and its NN O_6 layer, and class C3 includes four ILMEPs for the diffusion between two NN O_6 layers through a Li_2Ti_4 layer. Therefore, C1, C2, and C3 can be also more informatively denoted as $\{\text{Li}_6\text{-Li}_6\}$, $\{\text{Li}_6\text{-O}_6\}$, and $\{\text{O}_6\text{-Li}_2\text{Ti}_4\text{-O}_6\}$, respectively. Below, we describe these local diffusion paths in detail.

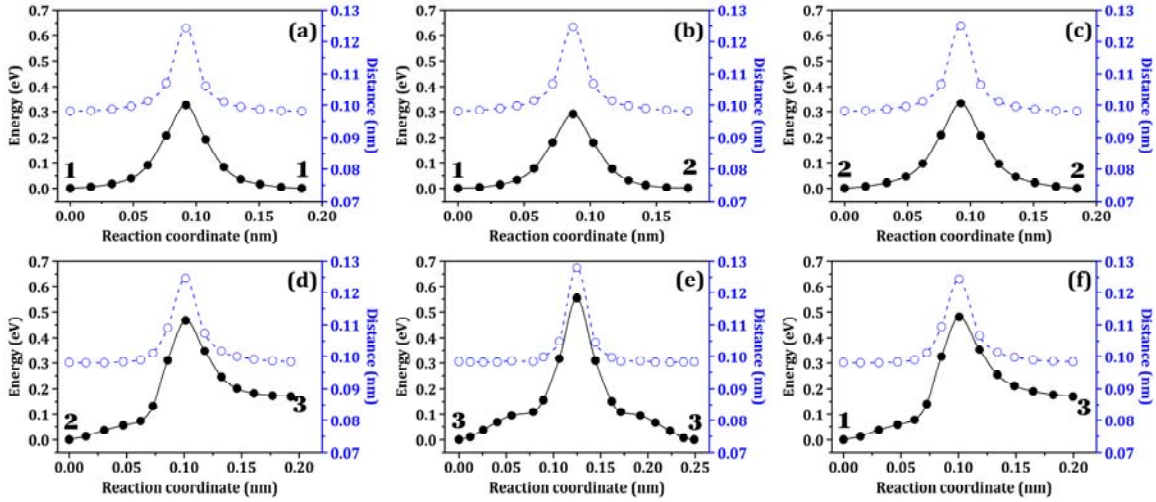
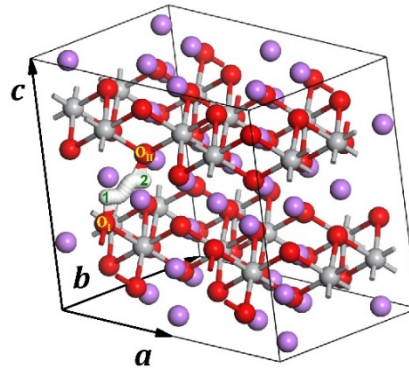


FIG. 3. Six ILMEPs (solid black curves) for class C1, or $\{\text{Li}_6\text{-Li}_6\}$, from our DFT calculations: (a) $1 \leftrightarrow 1$, (b) $1 \leftrightarrow 2$, (c) $2 \leftrightarrow 2$, (d) $2 \leftrightarrow 3$, (e) $3 \leftrightarrow 3$, and (f) $3 \leftrightarrow 1$. The corresponding cNEB trajectories of atoms are shown in Figs. 4 and S2 [34]. Dots represent cNEB images, and the corresponding curves are generated from a modified Bézier method [42] by fitting the data points versus reaction coordinates. A dashed blue curve with circles indicates the corresponding distance $d_{\text{O-T}}$ between the diffusing tritium and its nearby O atom. Similar statement applies for other MEP

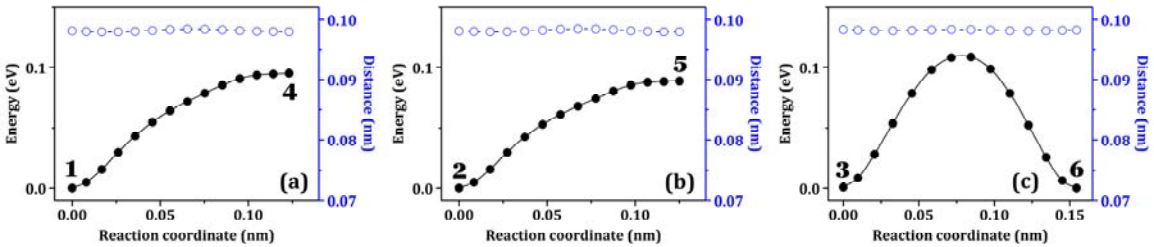


figures below.

FIG. 4. The trajectories of atoms from our cNEB calculation for the edge $1 \leftrightarrow 2$ in Fig. 3. The tritium (white ball) and two nearby O atoms (O_I and O_{II}) are indicated.

Class C1, or $\{\text{Li}_6\text{-Li}_6\}$, includes six ILMEPs between two NN T sites within the Li_6 layer (see Figs. 2(a) and 2(b)) corresponding to the six edges: $1\leftrightarrow 1$, $1\leftrightarrow 2$, $2\leftrightarrow 2$, $2\leftrightarrow 3$, $3\leftrightarrow 3$, and $3\leftrightarrow 1$, as plotted in Fig. 3. From these ILMEPs, the local diffusion barriers for class C1 can be obtained in the range from about 0.30 to 0.50 eV, which are listed in Table 2. We also notice that the barriers for $1\leftrightarrow 1$, $1\leftrightarrow 2$, and $2\leftrightarrow 2$ are significantly lower than $2\leftrightarrow 3$, $3\leftrightarrow 3$, and $3\leftrightarrow 1$. In Sec. III C, we will make more description for these barriers.

To trace the movement of a diffusing tritium and surrounding O atoms during the diffusion, in Fig. 3 we also plot the distance $d_{\text{O-T}}$ between the tritium and its NN O atom, as indicated by the dashed blue curve for each ILMEP. In Fig. 4, we show the trajectories of atoms from our cNEB calculation, taking the diffusion for edge $1\leftrightarrow 2$ as a typical example. For trajectories corresponding to all cNEB curves in Fig. 3, also see Fig. S2 [34]. From Fig. 3, it is obvious that the curve of $d_{\text{O-T}}$ always has the similar profile to the corresponding ILMEP, i.e., the larger $d_{\text{O-T}}$ corresponds to the higher energy. By checking the cNEB images, we find that the saddle point of an ILMEP is always approximately at the midpoint between two nearby O atoms (e.g., O_I and O_II for the edge $1\leftrightarrow 2$, as in Fig. 4), where $d_{\text{O-T}}$ is largest (i.e., farthest distance from both two nearby O atoms). This indicates that the saddle point is also a transition point of the bonding of tritium with its two nearby O atoms (e.g., the transition from the T-O_I to T-O_II bonding occurs at the midpoint between O_I and O_II



for the edge $1\leftrightarrow 2$ in Fig. 4). During the transition, the distance $d_{\text{O-T}}$ is significantly beyond the normal T-O bond length of about 0.098 nm (see Table 1), indicating that the T-O bond is broken. As an aside, the Ti-O bonds near the tritium also have corresponding significant relaxations during the diffusion process.

FIG. 5. Three ILMEPs (solid black curves with dots) for class C2, or $\{\text{Li}_6\text{-O}_6\}$, from our DFT calculations: (a) $1\leftrightarrow 4$, (b) $2\leftrightarrow 5$, and (c) $3\leftrightarrow 6$. The corresponding cNEB trajectories of atoms are shown in Figs. 6 and S3 [34]. A dashed blue curve with circles indicates the corresponding distance $d_{\text{O-T}}$ between the diffusing tritium and

its nearby O atom.

Class C2, or $\{\text{Li}_6\text{-O}_6\}$, includes three ILMEPs between a Li_6 -layer T site and its NN O_6 -layer T site (see Fig. 2(a)) corresponding to the three edges: $1\leftrightarrow 4$, $2\leftrightarrow 5$, and $3\leftrightarrow 6$, as plotted in Fig. 5. The diffusion process for each of these three edges turns out to be a simple rotation of the tritium around a nearby O atom, e.g., the rotation is around O_{II} for the edge $2\leftrightarrow 5$, as shown by the trajectories of atoms in Fig. 6. During the rotation, the distance $d_{\text{O-T}}$ between the tritium and its nearby O atom

approximately keeps the constant of about 0.098 nm. For trajectories corresponding to all cNEB curves in Fig. 5, also see Fig. S3 [34].

From the ILMEPs in Fig. 5, the PES near the T site 4 or site 5 is very flat so that the tritium does not relax to the energy minimum at site 1 or site 2 when any separate relaxation for the tritium initially placed near the site 4 or site 5 is performed. Thus, we also identify these two sites to be T sites, as already mentioned in Secs. II and III A.

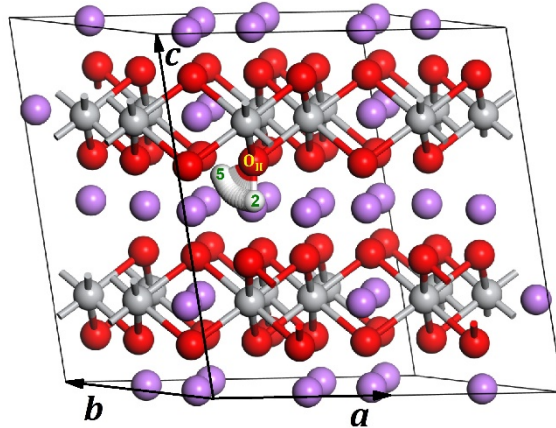


FIG. 6. The trajectories of atoms from our cNEB calculation for the edge $2\leftrightarrow 5$ in Fig. 5(b). The tritium (white ball) and its nearby O_{II} atom are indicated.

TABLE II. ILMEP classes and DFT energy barriers of tritium diffusion in the Li_2TiO_3 crystal. An arrow in the second column indicates the direction of local diffusion for an edge. The distance between two T sites (as two cNEB endpoints) for a diffusion path is listed in the fourth column. For the ILMEP curves corresponding to classes C1, C2, and C3, see Figs. 3, 5, and 7, respectively.

Class and notation	Edge and diffusion direction	Diffusion barrier (eV)	Distance (nm)
C1 $\{\text{Li}_6\text{-Li}_6\}$	$1\leftrightarrow 1$	0.326	0.1683
	$1\rightarrow 2$ ($1\leftarrow 2$)	0.291 (0.289)	0.1585
	$2\leftrightarrow 2$	0.333	0.1691

	2→3 (2←3)	0.467 (0.297)	0.1734
	3↔3	0.554	0.2045
	3→1 (3←1)	0.311 (0.481)	0.1799
C2 {Li ₆ -O ₆ }	1→4 (1←4)	0.095 (0.000)	0.1153
	2→5 (2←5)	0.089 (0.000)	0.1154
	3→6 (3←6)	0.109 (0.110)	0.1412
C3 {O ₆ -Li ₂ Ti ₄ -O ₆ }	6↔6	0.968	0.2771
	5↔5	1.005	0.3089
	5→4 (5←4)	0.916 (0.911)	0.3123
	4→6 (4←6)	0.934 (0.860)	0.2963

From Fig. 5 and Table 2, the energy barriers for class C2 are significantly smaller than those for class C1. Note that class C2 only includes three ILMEPs: 1↔4, 2↔5, and 3↔6. From our extensive cNEB calculations, we find that any of the MEPs for other six edges (i.e., 1↔5, 1↔6, 2↔4, 2↔6, 3↔4, and 3↔5) between a Li₆-layer T site and its NN O₆-layer T site is dependent, e.g., the MEP for 1↔5 is found to be the same as that for 1↔2↔5 (i.e., the combination of 1↔2 in C1 and 2↔5 in C2) after a cNEB calculation with two endpoints to be site 1 and site 5 is performed. This indicates that there is no straightforward diffusion for any of the above six edges, i.e., the diffusing tritium has to take a detour connected by the ILMEPs in C1 and C2. Similarly, the MEPs for 1↔6, 2↔4, 2↔6, 3↔4, and 3↔5 between a Li₆-layer T site (1, 2, or 3) and its NN O₆-layer T site (4, 5, or 6) are found to be the same as those for 1↔3↔6, 2↔1↔4, 2↔3↔6, 3↔1↔4, and 3↔2↔5, respectively.

Class C3, or {O₆-Li₂Ti₄-O₆}, includes four ILMEPs between two NN O₆-layer T sites through a Li₂Ti₄ layer (see Fig. 2(a)) corresponding to the four edges: 4↔6, 5↔4, 5↔5, and 6↔6, as plotted in Fig. 7. From these ILMEPs, the local diffusion barriers for class C3 can be obtained to be around 0.9 to 1.0 eV, which are listed in Table 2. These barriers are significantly higher than those for class C1.

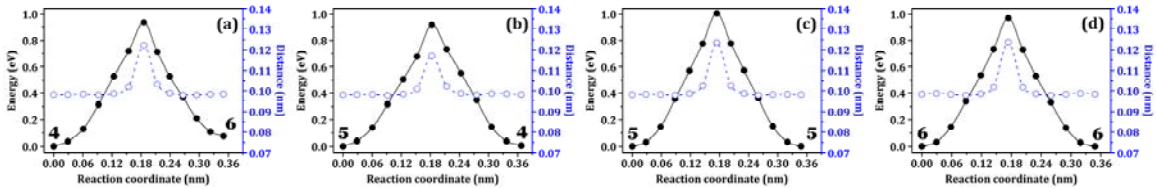


FIG. 7. Four ILMEPs (solid black curves with dots) for class C3, or {O₆-Li₂Ti₄-O₆}, from our DFT calculations: (a) 4↔6, (b) 4↔5, (c) 5↔5, and (d) 6↔6. The corresponding cNEB trajectories of atoms are shown in Figs. 8 and S4 [34]. A dashed blue curve with circles indicates the corresponding distance d_{O-T} between the

diffusing tritium and its nearby O atom.

Let us also trace the movement of a diffusing tritium and surrounding O atoms during the diffusion for C3. In Fig. 7, we plot the distance $d_{\text{O-T}}$ between the tritium and its NN O atom, as indicated by the dashed blue curve for each ILMEP. In Fig. 8, we show the trajectories of atoms from our cNEB calculation, taking the edge $6 \leftrightarrow 6$ as a typical example. For trajectories corresponding to all cNEB curves in Fig. 7, also see Fig. S4 [35]. From Fig. 7, it is obvious that the curve of $d_{\text{O-T}}$ always has the similar profile to the corresponding ILMEP, i.e., the larger $d_{\text{O-T}}$ corresponds to the higher energy. By checking the cNEB images, we find that the saddle point of an ILMEP is always approximately at the midpoint between two nearby O atoms (e.g., two O_{III} atoms in the NN O_6 -layer for $6 \leftrightarrow 6$, as in Fig. 8), where $d_{\text{O-T}}$ is largest (i.e., farthest distance from both two nearby O atoms). Therefore, the behavior of the trajectories of atoms for C3 is similar to that for C1, i.e., the saddle point is the transition point of the bonding of tritium with its two nearby O atoms, and the T-O bond is broken during the transition from the first T-O bonding to the second T-O bonding.

For the diffusion between two NN O_6 -layer T sites through a Li_2Ti_4 layer, there are six possible edges, four of which are included in class C3, as discussed above. From our cNEB calculations, the MEPs for other two possible edges (i.e., $4 \leftrightarrow 4$ and $5 \leftrightarrow 6$) are found to be dependent, being the combinations of some specific ILMEPs in classes C1, C2, and C3. The MEP for $5 \leftrightarrow 6$ is found to be the same as that for $5 \leftrightarrow 2 \leftrightarrow 2 \leftrightarrow 3 \leftrightarrow 6 \leftrightarrow 6$ (i.e., the combination of $5 \leftrightarrow 2$ in C2, $2 \leftrightarrow 2$ in C1, $2 \leftrightarrow 3$ in C1, $3 \leftrightarrow 6$ in C2, and $6 \leftrightarrow 6$ in C3), and similarly the MEP for $4 \leftrightarrow 4$ is found to be the same as that for $4 \leftrightarrow 1 \leftrightarrow 2 \leftrightarrow 2 \leftrightarrow 5 \leftrightarrow 4$.

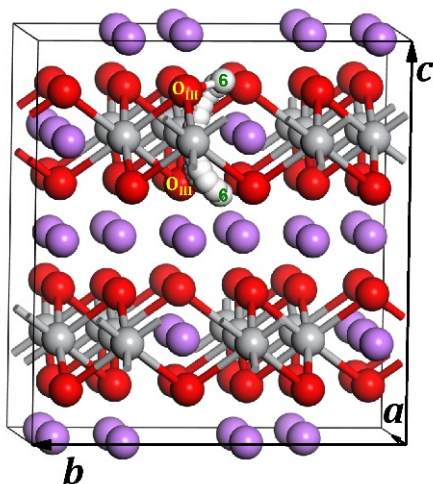


FIG. 8. The trajectories of atoms from our cNEB calculation for the diffusion path $6 \leftrightarrow 6$ in Fig. 7(d). The tritium (white ball) and its nearby O_{III} atoms are indicated.

Finally, it must be mentioned that we also perform extensive cNEB calculations for the edges from the T sites (4, 5, and 6) within an O_6 layer. We find that all MEPs for these edges are dependent, being the combinations of some ILMEPs in C1 and C2. For example, the MEPs for the shortest edges $4 \leftrightarrow 5$, $4 \leftrightarrow 6$, and $5 \leftrightarrow 6$ within an O_6 layer are found to be the same as those for $4 \leftrightarrow 1 \leftrightarrow 2 \leftrightarrow 2 \leftrightarrow 5$, $4 \leftrightarrow 1 \leftrightarrow 2 \leftrightarrow 3 \leftrightarrow 6$, and $5 \leftrightarrow 2 \leftrightarrow 2 \leftrightarrow 3 \leftrightarrow 6$, respectively. This indicates that the diffusion between two T sites within an O_6 layer has no straightforward way, the diffusing tritium having to make a detour via its nearby Li_6 -layer T sites for completing the diffusion process.

C. Long-range global anisotropic diffusion barriers

From Table 2, the short-range local diffusion processes of tritium for classes C1 and C2 have lower energy barriers than class C3, and therefore the diffusion rate within a Li_6 layer is much larger than those crossing a Li_2Ti_4 layer. This reveals the strong anisotropy of the tritium diffusion in the Li_2TiO_3 crystal. For clarity, in Fig. 9(a) we plot an energetically most favorable long-range diffusion path, which links the lowest-energy T sites 1 and 2 forming a zigzag chain along the $\langle 110 \rangle$ direction within a Li_6 layer (see the inset). The global diffusion barrier along the zigzag chain is 0.334 eV, which is at the saddle point for edge $2 \leftrightarrow 2$. Note that, within a Li_6 layer, the zigzag chains form an array alternatively with the rows of T sites 3 between these chains. The diffusion from the T site 1 or 2 towards 3 is more difficult due to the larger barriers 0.481 eV for $1 \rightarrow 3$ and 0.467 eV for $2 \rightarrow 3$. Also, the energy at T site 3 is about 0.17 eV higher than T sites 1 and 2, and thus each row of T sites 3 behaves like a ridge, while each zigzag chain behaves like a ditch on the PES. We also note that, except for the straightforward ILMEP in Fig. 3(e), the edge $3 \leftrightarrow 3$ corresponds to the dependent MEPs: $3 \leftrightarrow 2 \leftrightarrow 1 \leftrightarrow 3$ and $3 \leftrightarrow 2 \leftrightarrow 2 \leftrightarrow 1 \leftrightarrow 1 \leftrightarrow 3$ (also see Fig. 2(b)) with a global barrier of 0.481 eV (which equals the barrier for edge $1 \rightarrow 3$, see Table 2). This global barrier 0.481 eV is lower than the barrier of 0.554 eV from the ILMEP of $3 \leftrightarrow 3$ in Fig. 3(e), and therefore these dependent MEPs are more favorable but the diffusion paths are longer.

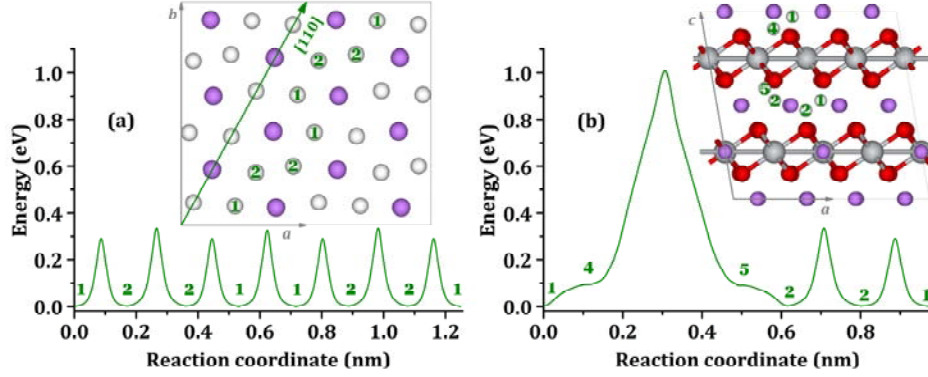


FIG. 9. (a) Most favorable cNEB diffusion path of tritium in Li_2TiO_3 crystal: $\dots \leftrightarrow 1 \leftrightarrow 2 \leftrightarrow 2 \leftrightarrow 1 \leftrightarrow 1 \leftrightarrow 2 \leftrightarrow 2 \leftrightarrow 1 \leftrightarrow \dots$, which is along the $\langle 110 \rangle$ direction within a Li_6 layer, as indicated by green number labels in the inset (for more details of the inset, also see Fig. 2(b)). (b) A most favorable cNEB MEP for tritium diffusion between two NN T sites 1 crossing an $\text{O}_6\text{-Li}_2\text{Ti}_4\text{-O}_6$ layer: $1 \leftrightarrow 4 \leftrightarrow 5 \leftrightarrow 2 \leftrightarrow 2 \leftrightarrow 1$, as indicated by green number labels in the inset.

In Fig. 9(b), we plot an energetically most favorable diffusion path between two T sites 1 crossing an $\text{O}_6\text{-Li}_2\text{Ti}_4\text{-O}_6$ layer. For the diffusion from the upper T site 1 in the inset of Fig. 9(b) to the lower T site 1 (i.e., correspondingly from left to right for the MEP curve in Fig. 9(b)), the tritium first makes a rotation from 1 to 4, then crosses the Li_2Ti_4 layer from 4 to 5, then make another rotation from 5 to 2, then undergoes two T sites 2, and finally arrives at the lower site 1. The global diffusion barrier of the path $1 \leftrightarrow 4 \leftrightarrow 5 \leftrightarrow 2 \leftrightarrow 2 \leftrightarrow 1$ is 1.006 eV, which is the sum of the barriers for edges $1 \rightarrow 4$ and $4 \rightarrow 5$ (see Table 2). Therefore, the global energy barrier (1.006 eV) for crossing a Li_2Ti_4 layer along the $\langle 001 \rangle$ direction is much larger than that (0.334 eV) for diffusing within a Li_6 layer along $\langle 110 \rangle$ direction. Similar to Fig. 9(b), any long-range diffusion paths along other crystalline directions can be analyzed by connecting the ILMEPs obtained in Sec. III B. Here we need to mention that, for the diffusion crossing an $\text{O}_6\text{-Li}_2\text{Ti}_4\text{-O}_6$ layer (as in Fig. 9), from our cNEB calculations we also find other shorter-range (or more straightforward) MEPs, which however have much larger global energy barriers (in the range of about 1.3 to 1.7 eV) and therefore these MEPs are unfavorable relative to the above most favorable path with the barrier of 1.006 eV.

As stated in Sec. I, the tritium diffusion barriers estimated from experiments have a considerable uncertainty in the range of 0.4 to 1.6 eV [11-17], which is reasonably consistent with our above DFT values, considering the various Li_2TiO_3 samples with different grain sizes, grain densities, grain orientations, defects, etc. in these experiments versus the perfect single Li_2TiO_3 crystal in this work. The existence of grains and defects in the crystal can make the system more isotropic, and then the corresponding lower limit of diffusion barriers should be significantly higher than 0.334 eV for the most favorable diffusion path within the Li_6 layer of a

perfect single crystal, for which the diffusivity of tritium is actually strongly anisotropic. Finally, we should also mention that the results from DFT rely on the validity of a GGA functional used in the calculations. The global barriers estimated from the hybrid functional PBE0 with exact exchange interaction [43] have an increasing of around 0.1 eV relative to the above PBE results. For details, see Sec. S3 [34].

IV. CONCLUSION

The diffusion of a positively-charged tritium interstitial in the perfect single Li_2TiO_3 crystal has been systematically studied. Various local diffusion paths and energy barriers between locally-stable sites of the tritium in the crystal have been obtained from our extensive DFT calculations incorporating the cNEB method. We find that the most favorable diffusion paths with a global energy barrier of 0.334 eV are along the $\langle 110 \rangle$ direction within the Li_6 layers, and the barrier crossing the $\text{O}_6\text{-Li}_2\text{Ti}_4\text{-O}_6$ layers for most favorable diffusion paths is 1.006 eV, revealing the strong anisotropy of the tritium diffusivity in the Li_2TiO_3 crystal. These theoretical predictions can provide important instructions for optimizing tritium extraction efficiency, and the energetic values obtained from this work can be the key parameter inputs in further lattice-gas modeling and kinetic Monte Carlo simulations for the temperature-dependent migration behavior of tritium in the Li_2TiO_3 crystal.

ACKNOWLEDGMENT

Y. S., J. Q., and T. L. acknowledge support from the National Magnetic Confinement Fusion Science Program (2014GB125002) and the National Natural Science Foundation of the People's Republic of China (number 11145006 and number 91326103). Y. H. was supported for this work by the U. S. Department of Energy (USDOE), Office of Science, Basic Energy Sciences, Materials Sciences and Engineering Division. His work was performed at Ames Laboratory which is operated by Iowa State University under Contract No. DE-AC02-07CH111358. The DFT calculations used resources of the National Energy Research Scientific Computing Center (NERSC), a U.S. DOE Office of Science User Facility operated under Contract No. DE-AC02-05CH11231, and used the Extreme Science and Engineering Discovery Environment (XSEDE), which is supported by National Science Foundation grant number ACI-1548562.

References:

- [1] M. Kikuchi, K. Lackner, and M. Q. Tran, *Fusion Physics* (IAEA, Vienna, 2012).
- [2] C. E. Johnson, K. Noda, and N. Roux, Ceramic breeder materials: Status and needs, *J. Nucl. Mater.* **258-263**, 140 (1998).

- [3] A. Ying, M. Akiba, L. V. Boccaccini, S. Casadio, G. Dell'Orco, M. Enoeda, K. Hayashi, J. B. Hegeman, R. Knitter, J. van der Laan, J. D. Lulewicz, and Z. Y. Wen, Status and perspective of the R&D on ceramic breeder materials for testing in ITER, *J. Nucl. Mater.* **367-370**, 1281 (2007).
- [4] Y. Duan and K. Parlinski, Density functional theory study of the structural, electronic, lattice dynamical, and thermodynamic properties of Li_4SiO_4 and its capability for CO_2 capture, *Phys. Rev. B* **84**, 104113 (2011).
- [5] P. Garin, E. Diegele, R. Heidinger, A. Ibarra, S. Jitsukawa, H. Kimura, A. Möslang, T. Muroga, T. Nishitani, Y. Poitevin, M. Sugimoto, and M. Zmitko, IFMIF specifications from the users point of view, *Fusion Eng. Des.* **86**, 611 (2011).
- [6] R. Knitter, P. Chaudhuri, Y. J. Feng, T. Hoshino, and I. K. Yu, Recent developments of solid breeder fabrication, *J. Nucl. Mater.* **442**, S420 (2013).
- [7] S. Konishi, M. Enoeda, M. Nakamichi, T. Hoshino, A. Ying, S. Sharafat, and S. Smolentsev, Functional materials for breeding blankets-status and developments, *Nucl. Fusion* **57**, 092014 (2017).
- [8] C. E. Johnson, Tritium behavior in lithium ceramics, *J. Nucl. Mater.* **270**, 212 (1999).
- [9] P. Bertone, The kinetics that govern the release of tritium from neutron-irradiated lithium oxide, *J. Nucl. Mater.* **151**, 281 (1988).
- [10] D. Zhu, T. Oda, Y. Shono, and S. Tanaka, Release behavior of hydrogen isotopes thermally sorbed in Li_2TiO_3 single crystal, *J. Nucl. Mater.* **442**, 437 (2013).
- [11] M. Kobayashi, Y. Oya, and K. Okuno, Migration of hydrogen isotopes in lithium metatitanate, *J. Nucl. Mater.* **439**, 159 (2013).
- [12] T. Kinjyo, M. Nishikawa, M. Enoeda, and S. Fukada, Tritium diffusivity in crystal grain of Li_2TiO_3 and tritium release behavior under several purge gas conditions, *Fusion Eng. Des.* **83**, 580 (2008).
- [13] T. Tanifuji, D. Yamaki, S. Nasu, and K. Noda, Tritium release behavior from neutron-irradiated Li_2TiO_3 single crystal, *J. Nucl. Mater.* **258-263**, 543 (1998).
- [14] M. Kobayashi, K. Kawasaki, T. Fujishima, Y. Miyahara, Y. Oya, and K. Okuno, Release kinetics of tritium generated in lithium-enriched $\text{Li}_{2+x}\text{TiO}_3$ by thermal neutron irradiation, *Fusion Eng. Des.* **87**, 471 (2012).
- [15] T. V. Kulsartov, Y. N. Gordienko, I. L. Tazhibayeva, E. A. Kenzhin, N. I. Barsukov, A. O. Sadvakasova, A. V. Kulsartova, and Z. A. Zaurbekova, Tritium migration in the materials proposed for fusion reactors: Li_2TiO_3 and beryllium, *J. Nucl. Mater.* **442**, 740 (2013).
- [16] S. Casadio, J. G. van der Laan, C. Alvani, A. J. Magielsen, and M. P. Stijkel, Tritium

- release kinetics from Li_2TiO_3 pebbles as prepared by soft-wet-chemistry, *J. Nucl. Mater.* **329-333**, 1252 (2004).
- [17] C. Alvani, St. Casadio, and S. Casadio, Kinetics of tritium release from irradiated Li_2TiO_3 pebbles in out-of-pile TPD tests, *Fusion Eng. Des.* **69**, 275 (2003).
- [18] I. R. Shein, T. A. Denisova, Y. V. Baklanova, and A. L. Ivanovskii, Structural, electronic properties and chemical bonding in protonated lithium metallates $\text{Li}_{2-x}\text{H}_x\text{MO}_3$ ($M = \text{Ti, Zr, Sn}$), *J. Struct. Chem.* **52**, 1043 (2011).
- [19] V. M. Zainullina, V. P. Zhukov, T. A. Denisova, and L. G. Maksimova, Electronic structure and chemical bonding in monoclinic and cubic $\text{Li}_{2-x}\text{H}_x\text{TiO}_3$ ($0 \leq x \leq 2$), *J. Struct. Chem.* **44**, 180-186 (2003).
- [20] S. T. Murphy, Tritium Solubility in Li_2TiO_3 from First-Principles Simulations, *J. Phys. Chem. C* **118**, 29525 (2014).
- [21] M. Oyaidzu, Y. Morimoto, H. Kodama, M. Sasaki, H. Kimura, K. Munakata, M. Okada, K. Kawamoto, H. Moriyama, M. Nishikawa, and K. Okuno, Correlation between annihilation of radiation defects and tritium release in Li_2TiO_3 , *J. Nucl. Mater.* **329-333**, 1313 (2004).
- [22] L. Padilla-Campos, Theoretical study of two possible occupation sites for tritium atoms in lithium titanate, *J. Mol. Struct. (Theochem)* **580**, 101 (2002).
- [23] L. Padilla-Campos, A theoretical investigation of occupation sites for tritium atoms in lithium titanate, *J. Mol. Struct. (Theochem)* **621**, 107 (2003).
- [24] B. Ruprecht, M. Wilkening, R. Uecker, and P. Heitjans, Extremely slow Li ion dynamics in monoclinic Li_2TiO_3 —probing macroscopic jump diffusion via ^7Li NMR stimulated echoes, *Phys. Chem. Chem. Phys.* **14**, 11974 (2012).
- [25] M. Vijayakumar, S. Kerisit, Z. Yang, G. L. Graff, J. Liu, J. A. Sears, S. D. Burton, K. M. Rosso, and J. Hu, Combined $^6,^7\text{Li}$ NMR and Molecular Dynamics Study of Li Diffusion in Li_2TiO_3 , *J. Phys. Chem. C* **113**, 20108 (2009).
- [26] G. Henkelman, B. P. Uberuaga, and H. Jónsson, A climbing image nudged elastic band method for finding saddle points and minimum energy paths, *J. Chem. Phys.* **113**, 9901 (2000).
- [27] G. Henkelman and H. Jónsson, Improved tangent estimate in the nudged elastic band method for finding minimum energy paths and saddle points, *J. Chem. Phys.* **113**, 9978 (2000).
- [28] K. Kataoka, Y. Takahashi, N. Kijima, H. Nagai, J. Akimoto, Y. Idemoto, and K. Ohshima, Crystal growth and structure refinement of monoclinic Li_2TiO_3 , *Mater. Res. Bull.* **44**, 168 (2009).
- [29] N. V. Tarakina, R. B. Neder, T. A. Denisova, L. G. Maksimova, Y. V. Baklanova, A. P.

Tyutyunnik, and V. G. Zubkov, Defect crystal structure of new $\text{TiO}(\text{OH})_2$ hydroxide and related lithium salt Li_2TiO_3 , Dalton Trans. **39**, 8168 (2010).

[30] G. Kresse and J. Hafner, *Ab initio* molecular dynamics for liquid metals, Phys. Rev. B **47**, 558 (1993).

[31] G. Kresse and J. Furthmüller, Efficient iterative schemes for *ab initio* total-energy calculations using a plane-wave basis set, Phys. Rev. B **54**, 11169 (1996).

[32] G. Kresse and D. Joubert, From ultrasoft pseudopotentials to the projector augmented-wave method, Phys. Rev. B **59**, 1758 (1999).

[33] J. P. Perdew, K. Burke, and M. Ernzerhof, Generalized Gradient Approximation Made Simple, Phys. Rev. Lett. **77**, 3865 (1996).

[34] See Supplemental Material at <http://link.aps.org/supplemental/xx.xxxx/PhysRevApplied.x.xxxxxx> for further details on testing system size and the number of cNEB images used to calculate diffusion barriers, the trajectories of atoms from our cNEB calculations for ILMEPs, and estimating diffusion barriers from the PBE0 functional.

[35] D. Marx, M. E. Tuckerman, J. Hutter, and M. Parrinello, The nature of the hydrated excess proton in water, Nature **397**, 601 (1999).

[36] D. M. Wilkins, D. E. Manolopoulos, S. Pipolo, D. Laage, and J. T. Hynes, Nuclear Quantum Effects in Water Reorientation and Hydrogen-Bond Dynamics, J. Phys. Chem. Lett. **8**, 2602 (2017).

[37] S. B. Zhang and J. E. Northrup, Chemical Potential Dependence of Defect Formation Energies in GaAs: Application to Ga Self-Diffusion, Phys. Rev. Lett. **67**, 2339 (1991).

[38] C. G. Van de Walle, D. B. Laks, G. F. Neumark, and S. T. Pantelides, First-principles calculations of solubilities and doping limits: Li, Na, and N in ZnSe, Phys. Rev. B **47**, 9425 (1993).

[39] C. Freysoldt, B. Grabowski, T. Hickel, J. Neugebauer, G. Kresse, A. Janotti, and C. G. Van de Walle, First-principles calculations for point defects in solids, Rev. Mod. Phys. **86**, 253 (2014).

[40] G. Henkelman, A. Arnaldsson, and H. Jónsson, A fast and robust algorithm for Bader decomposition of charge density, Comput. Mater. Sci. **36**, 254 (2006).

[41] B. S. Manoj, A. Chakraborty, and R. Singh, *Complex Networks: A Networking and Signal Processing Perspective*, (Pearson, New York, 2018).

[42] G. Farin, *Curves and Surfaces for CAGD: A Practical Guide*, 5th ed. (Academic, San Diego, 2002).

[43] J. P. Perdew, M. Ernzerhof, and K. Burke, Rationale for mixing exact exchange

with density functional approximations, J. Chem. Phys. **105**, 9982 (1996).